ACS APPLIED NANO MATERIALS

www.acsanm.org Article

ZnMgO Nanoparticles via Ultrasonic-Assisted Synthesis for Electron Transport Layer in InP-Based QD-LEDs

Hyeonseung Ban, Yeongho Choi, Hyo Geun Lee, Woon Ho Jung, Jaehoon Lim, and Seong-Yong Cho*

Cite This: ACS Appl. Nano Mater. 2024, 7, 11274−11284 Read Online

ACCESS | Metrics & More | Article Recommendations | Supporting Information

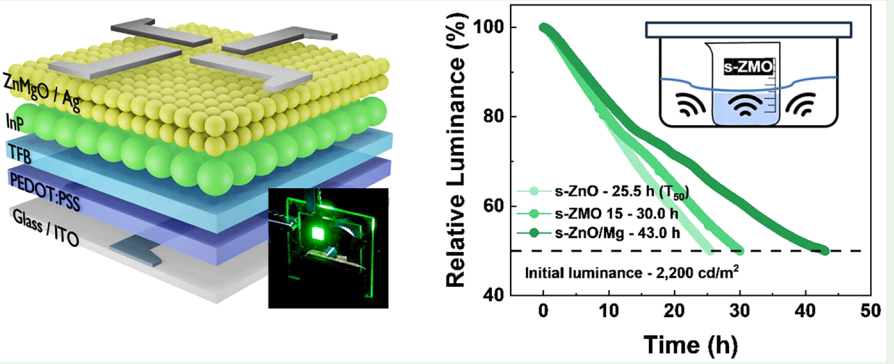

ABSTRACT: Ultrasonic-assisted synthesis was performed to effectively dope ZnO nanoparticles (NPs) with Mg for use in colloidal quantum dot light-emitting diodes (QD-LEDs). When ZnMgO NPs were synthesized through ultrasonic synthesis, higher Mg doping concentrations could be achieved, despite the smaller sizes of NPs than those synthesized using conventional heating methods. Additionally, to improve the stability of the electron transport layer (ETL) in the QD-LED structure, a ZnO/$Mg(OH)_2$ (s-ZnO/Mg) structure was synthesized by first synthesizing ZnO via ultrasonication, followed by Mg treatment. When s-ZnO/Mg was applied to a green-emitting InP QD-LED device, the brightness and efficiency of the device were significantly improved. Specifically, the green-emitting InP QD-LED device exhibited a luminance of 25,396 cd/m^2 and an external quantum efficiency (EQE) of 2.51%. These results represent a 1.32- and 1.43-fold increase in luminance and EQE, respectively, compared to the QD-LED device with ultrasound-assisted ZnO. During the lifetime measurement of the QD-LED device, it required approximately 43.0 h to reach half its brightness at a luminance of 2,200 cd/m^2, which is a 1.69-fold increase compared to the QD-LED device with ZnO.

KEYWORDS: *ZnMgO nanoparticles, colloidal quantum dot, light-emitting diodes, ultrasonic, $Mg(OH)_2$, doping*

INTRODUCTION

Quantum dot light-emitting diodes (QD-LED) are promising future emissive display devices owing to their high performance and solution processability.[1−3] In the early stages of QD-LED development, the device architecture was the same as that of an organic LED, in which several monolayers of QD film were sandwiched between organic charge transport layers (CTLs).[4,5] The device structure is complicated to minimize unwanted exciton quenching and provide a better charge balance during device operation.[6,7] The performance and lifetime of QD-LED devices have significantly improved by employing inorganic electron transport layers (ETLs).[8] Specifically, the device structure can be either standard (ITO/organic hole injection and transport layer/QD/ZnO/Al) or inverted (ITO/ZnO/QD/organic hole transport layer (HTL)/MoO_3/Al). The fact that both structures use a ZnO ETL indicates that ZnO is the best choice for QD-LED devices.[8−15]

Despite the significantly improved device performance of QD-LEDs using ZnO ETL, concerns remain regarding ZnO ETL. Relatively faster electron transport in ZnO compared to hole transport in organic HTL results in negative trion and nonradiative Auger recombination.[16,17] In addition, the negligible electron transport barrier at the conduction band edges contributes to the same effect, considering that there is a large hole injection barrier at the valence band edges of organic CTLs.[18−20] Therefore, researchers have attempted to dope ZnO with foreign elements to widen its electronic bandgap and reduce its electron mobility. Many elements (Al, Li, Ga, and Zr) have been doped for use in QD-LED devices;[21−27]

Received: February 7, 2024
Revised: April 25, 2024
Accepted: April 28, 2024
Published: May 6, 2024

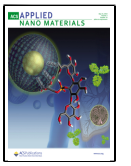

https://doi.org/10.1021/acsanm.4c00820
ACS Appl. Nano Mater. 2024, 7, 11274−11284

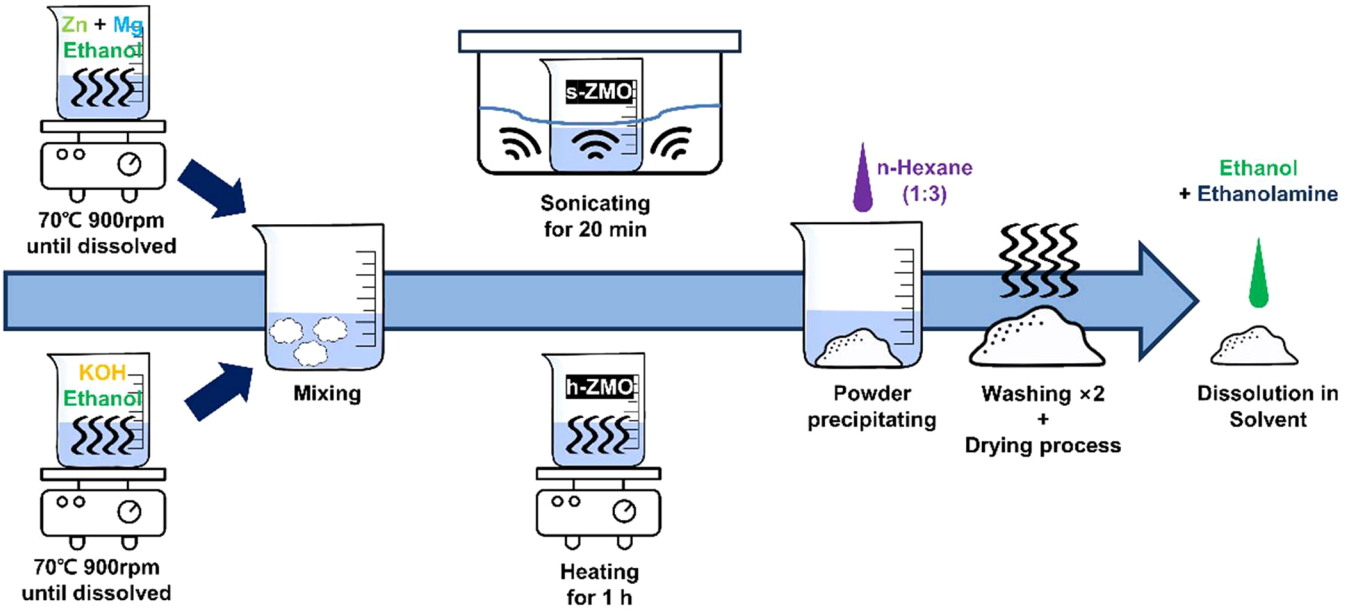

Figure 1. Schematic of ultrasonic-assisted and heating-assisted ZMO synthesis in this work and the purification method of ZMO NPs.

however, Mg-doped ZnO (ZnMgO or ZMO) is most frequently used because of its facile doping and high performance when ZMO is used as an ETL.[28] Tetramethylammonium hydroxide (TAMH) is frequently used to synthesize ZnO and ZMO nanoparticles (NPs) at room temperature. This is due to the different reactivities of the Mg and Zn precursors during ZMO synthesis at higher temperatures.[26] Specifically, a significantly smaller amount of Mg is observed after the synthesis of ZMO NPs.[29]

Here, ultrasonic-assisted synthesis of ZMO is reported for the first time for use as an ETL in QD-LED devices. Mg and Zn precursors were mixed in a cheaper and ecofriendly solvent (ethanol), and the reaction was initiated by adding a potassium hydroxide (KOH) solution. To promote the reaction rate and incorporation of Mg during ZMO synthesis, reaction precursors in solution were placed in an ultrasonic bath instead of simply stirring and heating. The ZMO NPs were successfully synthesized and dispersed in an alcohol. The optical bandgap of ZMO was gradually increased by doping with Mg, and we revealed that more Mg was incorporated into ZMO compared to the typical heating synthesis despite the same precursor ratio. The bandgap of ZMO prepared by the ultrasound-assisted method effectively increased owing to enhanced reactivity of Mg precursors and smaller physical size of ZMO compared with heating-assisted ZMO. When the particle size distribution of ZMO was confirmed, the ultrasonically synthesized ZMO formed a more uniform particle size.

A green-emitting InP-based QD-LED device was fabricated to test the effect of Mg doping in ZnO ETL, and a maximum luminance of 17,492 cd/m^2 and external quantum efficiency (EQE) of 2.07% were achieved. Furthermore, exploiting the enhanced ease of Mg incorporation through ultrasonic synthesis, we conducted the synthesis by coating the surface of ZnO NPs with $Mg(OH)_2$ to act as a passivation layer. When applied to green InP QD-LED devices, the maximum luminance and EQE value reached 25,396 cd/m^2 and 2.51%, showing a 1.32- and 1.43-fold efficiency boost compared with the QD-LED device with ZnO ETL. Additionally, the device lifetime exhibited a notable enhancement, with an efficiency increase of approximately 1.69 times, reaching 43 h from the onset of 2,200 cd/m^2 to T_{50}.

RESULTS AND DISCUSSION

ZMO NPs were synthesized by using KOH as the reactant in an ultrasonic bath. Two solutions containing zinc acetate dihydrate and magnesium acetate tetrahydrate in ethyl alcohol and KOH in ethyl alcohol were heated to 70 °C to dissolve each precursor separately as shown in Figure 1. Subsequently, the two solutions were mixed to react. When the mixture became transparent, ultrasonication was performed for 20 min to synthesize ZMO x (molar feeding ratio of Mg among cations) (x = 0, 5, 10, 15, and 20). Additionally, for comparison, ZMO NPs are synthesized by simply heating at 70 °C for 1 h without the aid of ultrasonic.[8,30] When ZnO NPs were synthesized by heating without adding Mg, the ZnO NPs precipitated after 1 h of synthesis, presumably because of their larger size. However, the addition of Mg resulted in the formation of smaller particles because of the low reactivity of the Mg precursor,[26] and natural precipitation did not occur, as shown in Figure S1a. To induce precipitation of ZMO NPs, *n*-hexane was added as an antisolvent in a 1:3 ratio to the synthesized solution (Figure S1b). The precipitated powder was purified twice using ethyl alcohol and *n*-hexane and then dried under vacuum to remove impurities and residual solvents. The purified powder was dissolved in ethyl alcohol at a ratio of 20 mg/mL, and ethanolamine was added to the ZMO solution as a stabilizer (Figure 1).[31] Each sample was synthesized using ultrasonic-assisted ZMO (s-ZnO, s-ZMO 5, s-ZMO 10, s-ZMO 15, and s-ZMO 20) and heating-assisted ZMO (h-ZnO, h-ZMO 10, and h-ZMO 15), depending on the synthesis method and Mg concentration. The amounts of Zn and Mg precursors for NP synthesis are listed in Table S1.

When comparing the absorbances of s-ZMO and h-ZMO, it was observed that in all samples, increasing the Mg concentration resulted in a blue-shifted peak (Figure 2a,b), which indicates a wider optical bandgap of ZMO. The optical

https://doi.org/10.1021/acsanm.4c00820
ACS Appl. Nano Mater. 2024, 7, 11274−11284

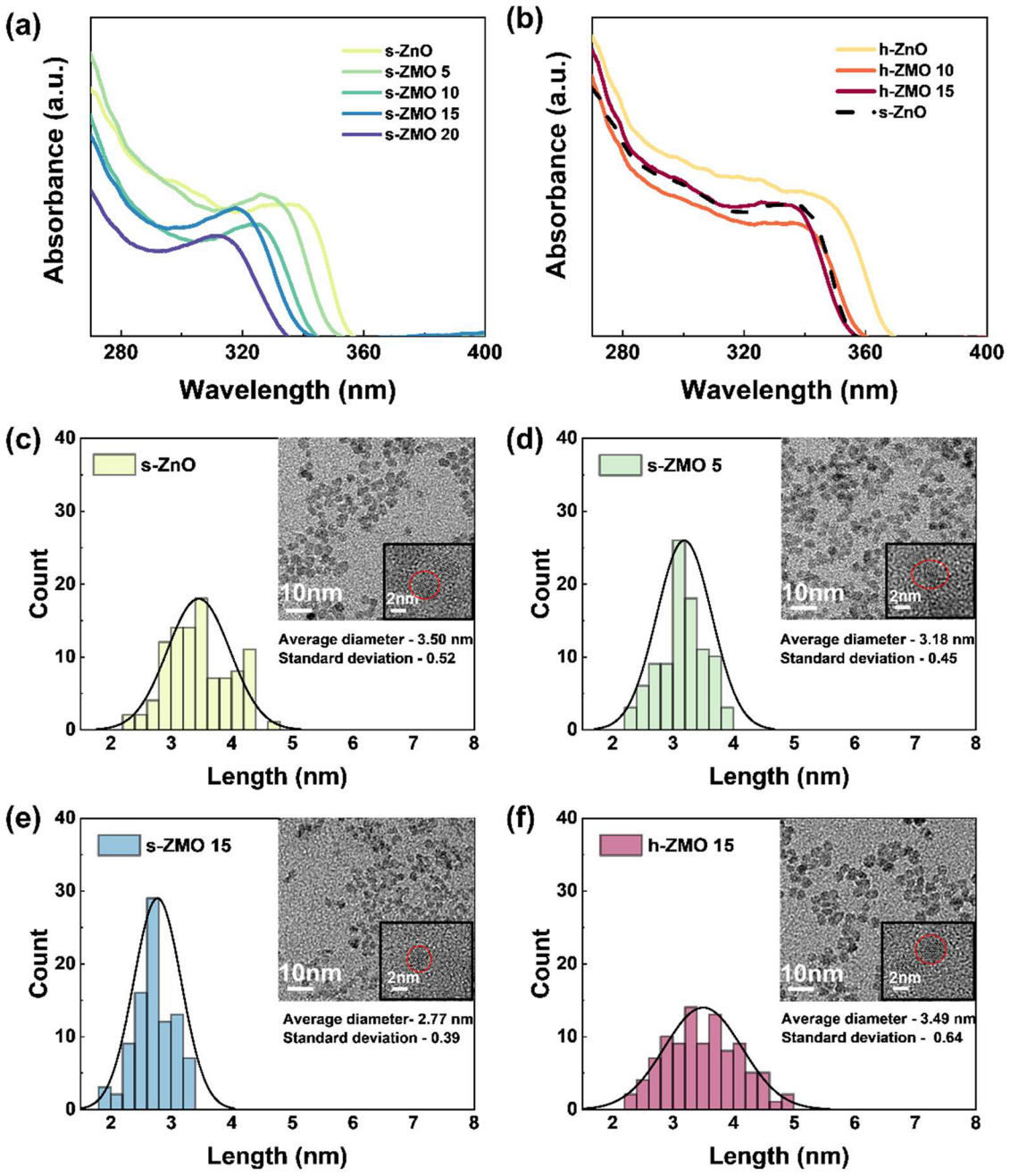

Figure 2. (a) Absorption spectrum of s-ZMO. (b) Absorption spectra of h-ZMO and s-ZnO. Particle size distribution histogram, Gaussian distribution, and low and high magnification. (insets) TEM images of (c) s-ZnO, (d) s-ZMO 5, (e) s-ZMO 15, and (f) h-ZMO 15.

bandgap values of ZMO NPs were determined from the absorption spectra using the Tauc equation.[32]

$$(\alpha h\nu)^2 = \text{const}(h\nu - E_g)$$

where α is the absorption coefficient, $h\nu$ the photon energy, and E_g the optical bandgap of ZMO.

The optical bandgap increased with increasing Mg content, and a higher value was observed for s-ZMO than for h-ZMO at the same concentration of Mg (Figure S2a,b) (s-ZnO: 3.534 eV; s-ZMO 5: 3.603 eV; s-ZMO 10: 3.669 eV; s-ZMO 15: 3.718 eV; s-ZMO 20: 3.785 eV; h-ZnO: 3.420 eV; h-ZMO 10: 3.516 eV; and h-ZMO 15: 3.551 eV). When an alloy is formed by adding Mg to ZnO, the energy level increases.[33] In addition, as the size of the ZMO NPs decreases, the optical bandgap is expected to increase owing to the quantum confinement effect.[34] Additionally, when the first exciton peaks in the absorption spectra are examined, the more prominent peak in s-ZMO compared with that in h-ZMO implies a comparatively consistent particle size. To elucidate the exact size of ZMO NPs and correlate the size of NPs with absorption spectra, transmission electron microscopy (TEM) analysis was performed, as shown in Figure 2c–f. Figure 2c–f shows the histogram and Gaussian distribution of each measured sample and the low- and high-magnification (insets) TEM images of s-ZnO, s-ZMO 5, s-ZMO 15, and h-ZMO 15. When confirming s-ZMO, the particle size gradually decreased with the amount of Mg doping (average diameter: s-ZnO: 3.50 nm; s-ZMO 5: 3.18 nm; s-ZMO 15: 2.77 nm), and h-ZMO 15 exhibited an

https://doi.org/10.1021/acsanm.4c00820
ACS Appl. Nano Mater. 2024, 7, 11274−11284

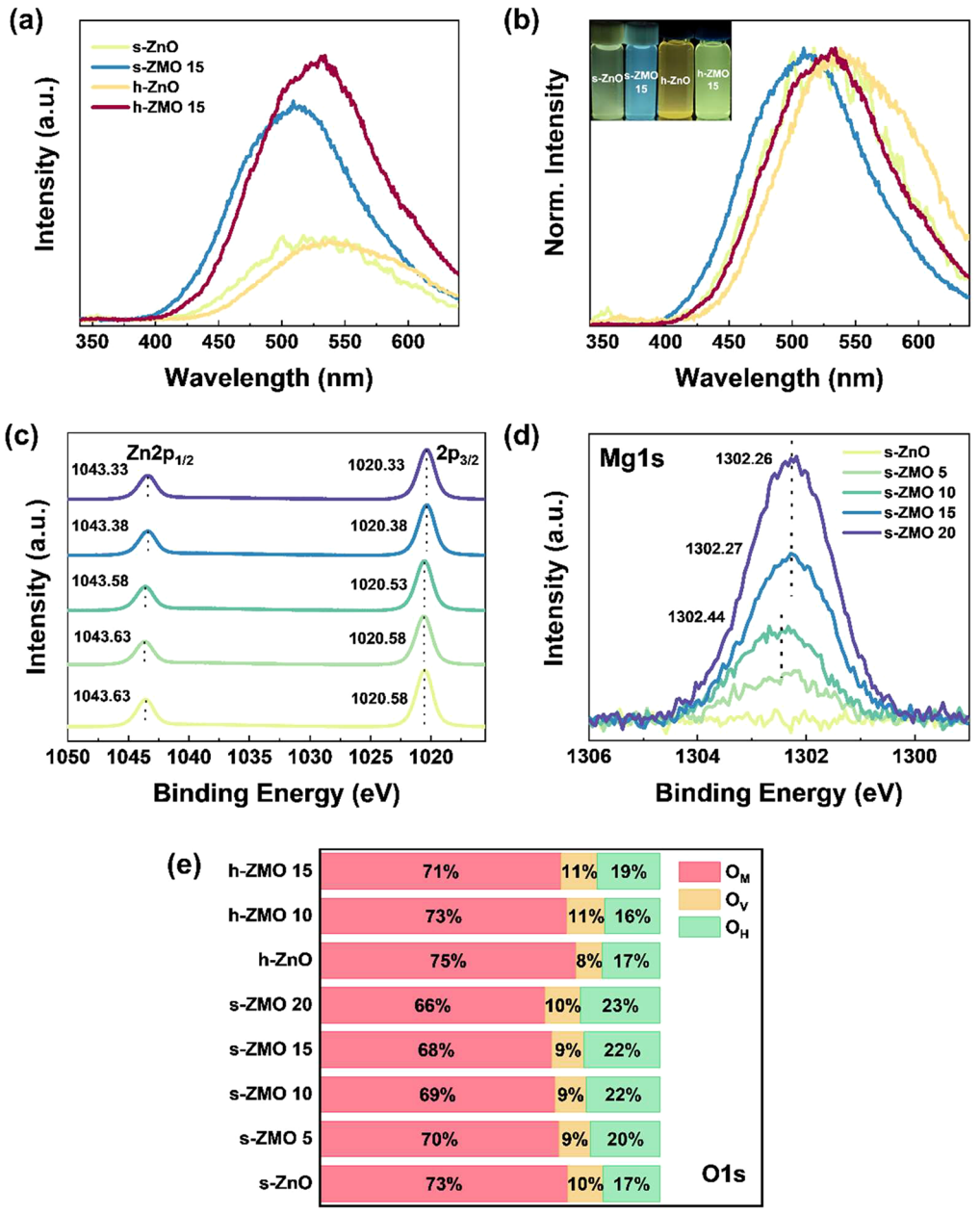

Figure 3. (a) PL spectra of s-ZnO, s-ZMO 15, h-ZnO, and h-ZMO 15. (b) Normalized PL spectra in the visible region and a photograph of the s-ZnO, s-ZMO 15, h-ZnO, and h-ZMO 15 under a 365 nm UV lamp (inset). (c) Zn 2p XPS spectra of s-ZMO. (d) Mg 1s XPS spectra of s-ZMO. (e) Ratio of divided O 1s peaks (O_M, O_V, and O_H) in s-ZMO and h-ZMO.

average size of 3.49 nm despite more added Mg. When comparing the same synthesis methods, it was observed that an increase in Mg content resulted in the formation of smaller particles owing to the lower reactivity of the Mg precursor. The standard deviations confirmed that s-ZMO exhibited a more uniform particle size distribution than h-ZMO (s-ZnO: 0.52; s-ZMO 5: 0.45; s-ZMO 15: 0.39; h-ZMO 15: 0.64). The uniformity in particle size of s-ZMO became more pronounced with the addition of Mg, as indicated by the increasingly homogeneous data.

The photoluminescence (PL) of ZnO can be categorized into UV and visible regions, where the UV region corresponds to the intrinsic wavelength of ZnO and the visible region is associated with wavelengths stemming from surface defects in ZnO. The PL spectra of ZMO were compared using representative samples, including s-ZnO, s-ZMO 15, h-ZnO, and h-ZMO 15. Figure 3a shows the measured PL spectral data, and Figure 3b displays the normalized data of the PL spectra in the visible region and a photograph of the ZMO solution under a 365 nm UV lamp. Analysis of the normalized PL data revealed that the wavelength in the visible region of ZMO underwent a blue-shift with the addition of Mg, exhibiting a trend similar to that of the absorption spectra. This shift was linked to an increase in the donor state level of defects as the size of the ZnO NPs decreased. The visible-light wavelength associated with surface defects in ZnO increased in intensity as the particle size decreased because of the increasing surface area.[34] However, despite the observed blue-shift in s-ZMO 15 compared to that in h-ZMO 15, a lower intensity was observed. Therefore, it can be inferred that ultrasonic synthesis resulted in the formation of ZMO with lower defect levels in comparison to the heat-assisted method.

https://doi.org/10.1021/acsanm.4c00820
ACS Appl. Nano Mater. 2024, 7, 11274−11284

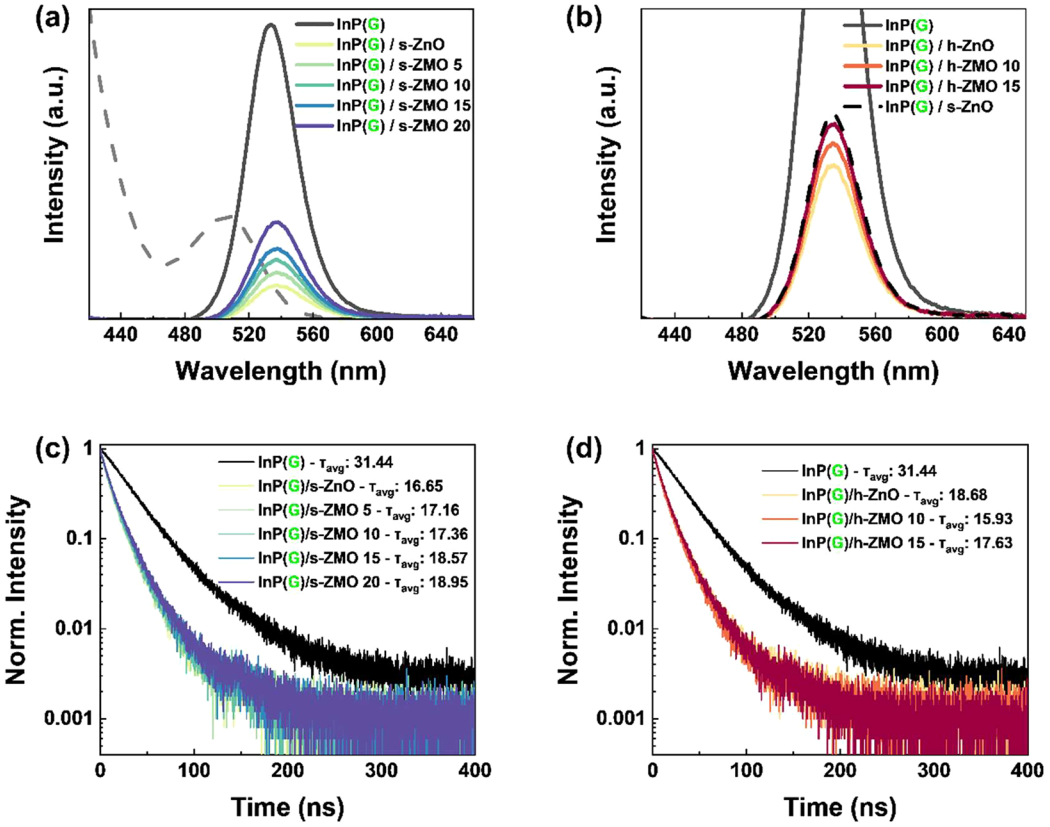

Figure 4. (a) PL and absorption spectra of glass/InP/s-ZMO. (b) PL spectra of glass/InP/h-ZMO or s-ZnO. (c) Time-resolved PL spectra of glass/InP/s-ZMO. (d) Time-resolved PL spectra of glass/InP/h-ZMO.

X-ray photoelectron spectroscopy (XPS) was conducted for quantitative analysis of Mg doping in ZMO. The actual Mg doping amount in all the samples was approximately half or less than the added Mg doping amount because of the lower reactivity of the Mg precursor, as summarized in Table S2. In addition, s-ZMO showed a higher Mg doping concentration than h-ZMO (Table S2) at the same Mg concentration, clearly indicating that ultrasonic treatment effectively enhances the reactivity of the Mg precursors. When synthesizing ZMO by heating, the increased diffusion of Zn^{2+} leads to the formation of relatively large and nonuniform particles.[34] When synthesized using ultrasonication, an instantaneous temperature of 5,000 K and pressure of 1,000 atm are generated, but the solution itself maintains room temperature because the cooling rate is 10^{10} K s^{-1}.[25] The momentary energy applied at room temperature is speculated to increase the doping ratio of Mg and suppress the diffusion of Zn^{2+}, resulting in the formation of ZMO nanoparticles with a higher Mg ratio and relatively smaller size. The Zn 2p binding energies (s-ZnO reference: Zn $2p_{1/2}$: 1043.63 eV; Zn $2p_{3/2}$: 1020.58 eV) represent Zn in ZMO, and this value exhibits a decrease in binding energy with increasing Mg doping (Figure 3c and Figure S3a). The Mg 1s binding energy, representing Mg, was not observed in s-ZnO and h-ZnO because of the absence of Mg doping; however, its intensity increased with an increase in Mg doping. Similar to the Zn 2p peak, this value exhibited a decrease in binding energy with increasing Mg doping (Figure 3d and Figure S3b). The shift toward lower binding energies of the Zn 2p and Mg 1s peaks is attributed to the influence of different metal ions (Zn and Mg) causing oxygen deficiency.[35] The O 1s peak, which represents the binding energy in the oxide region, can be divided into three main peaks. Specifically, the O_M peak is associated with bonding with metal ions, the O_V peak is related to oxygen vacancies, and the O_H peak corresponds to hydroxides.[28] The respective peaks were observed at 529.58, 531.03, and 531.57 eV for s-ZnO. In ZnO, the presence of O_V leads to intrinsic defects that cause exciton quenching between QD and ZnO in QD-LED structures.[22] The O_V peak showed little variation even with the doping of Mg (s-ZnO: 10.3%; s-ZMO 5: 9.3%; s-ZMO 10: 9.2%; s-ZMO 15: 9.4%; s-ZMO 20: 10.4%) (Figure S3c–g). h-ZMO exhibited a lower O_V peak than s-ZnO, but an increase in the peak was observed with increasing Mg doping (h-ZnO: 7.6%; h-ZMO 10: 11.0%; h-ZMO 15: 10.5%) (Figure S3h–j). The O_H peak of ZnO showed a slight decrease in h-ZMO 10, while both s-ZMO and h-ZMO exhibited an increasing trend with increasing Mg doping (s-ZnO: 16.8%; s-ZMO 5: 20.4%; s-ZMO 10: 21.7%; s-ZMO 15: 22.3%; s-ZMO 20: 23.4%; h-ZnO: 17.0%; h-ZMO 10: 16.3%; h-ZMO 15: 18.5%) (Figure 3e). The increase in the intensity of the O_H peak was attributed to an increase in $Mg(OH)_2$, similar to the observation of the Mg 1s peak. Both s-ZnO and h-ZnO showed a gradual decrease in the intensity of the O_M peak with increasing Mg concentration.

Before incorporating ZMO as an ETL in QD-LED devices, we deposited ZMO onto a QD film and examined the PL characteristics of the QDs. Environmentally friendly green-emitting InP QDs were used in this study. When s-ZMO was coated on the QD layer, the PL intensity decreased compared with that of the pristine QD film. However, as the Mg doping increased, the extent of PL quenching decreased (Figure 4a). Similar results were observed when h-ZMO was coated onto

https://doi.org/10.1021/acsanm.4c00820
ACS Appl. Nano Mater. 2024, 7, 11274−11284

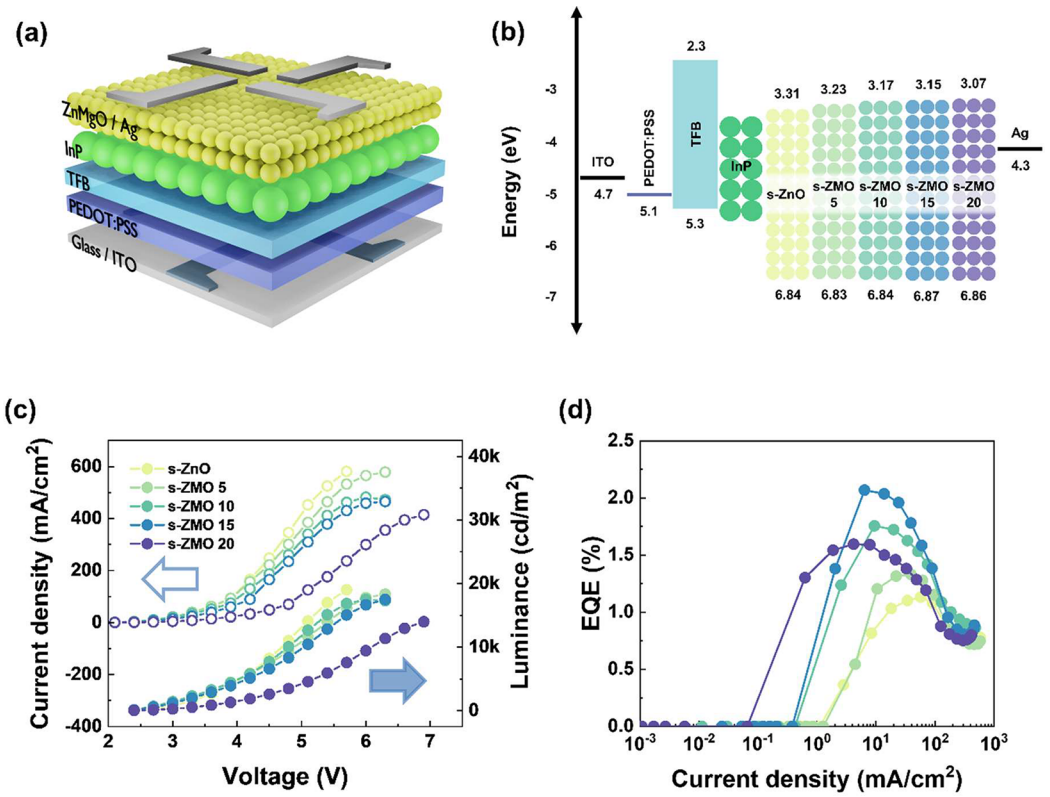

Figure 5. (a) Schematic of the QD-LED device, (b) expected energy band diagram, (c) J–V–L characteristics, and (d) EQE–current density of the green emitting InP QD-LED device with s-ZMO (0–20).

the QD layer (Figure 4b). The PL intensity of QD/s-ZnO was higher than the PL intensity of QD/h-ZMO 15. At the QD/ZMO interface, PL quenching can be attributed to surface defects or electron transfer owing to negligible barriers in the conduction band minimum (CBM).[36] The PL of QD/ZMO exhibited a reduced quenching intensity with higher optical bandgap values of ZMO, suggesting a strong association with electron transfer. Furthermore, time-resolved PL (TRPL) data for QD/ZMO were also recorded, revealing different patterns compared with PL results. Average PL lifetime was calculated by a triexponential fitting function (average PL lifetime τ (ns): reference −31.44; s-ZnO: 16.65; s-ZMO 5: 17.16; s-ZMO 10: 17.36; s-ZMO 15: 18.57; s-ZMO 20: 18.95; h-ZnO: 18.68; h-ZMO 10: 15.93; h-ZMO 15: 17.63) (Figure 4c,d and Table S3). For s-ZMO, as Mg doping increased, the quenching effect on the lifetime gradually diminished. Among the h-ZMO samples, h-ZnO exhibited the longest lifetime, whereas shorter lifetimes were observed when Mg was introduced. For h-ZMO 10 and 15, unlike s-ZMO, Mg doping significantly increased the number of surface defects, resulting in the strengthening of exciton traps within the defect region. Therefore, it was suggested that in contrast to the PL results, TRPL indicated an increased influence of surface defects. However, the discrepancy in TRPL based on the sample was minimal.

Electroluminescence (EL) devices were fabricated to evaluate the performance of s-ZMO in green-emitting InP QD-LED. The device structure consisted of a glass substrate, ITO as the anode, poly(ethylenedioxythiophene):polystyrenesulfonate (PEDOT:PSS) as the HIL, HTL as poly[(9,9-dioctylfluorenyl-2,7-diyl)-*co*-(4,4′-(*N*-(4-*s*-butylphenyl))-diphenylamine)] (TFB), green-emitting InP QD as the emitting layer (EML), ZMO (s-ZMO) as the ETL, and Ag as the cathode (Figure 5a). Figure 5b shows the energy-band diagrams of the green-emitting InP QD-LED functional layers and s-ZMO with varying Mg doping concentrations. Ultraviolet photoelectron spectroscopy (UPS) was performed to calculate the energy bandgap of s-ZMO. Figures S4a and S4b show the measured secondary electron cutoff (BE_{cutoff}) and valence band region (BE_{onset}) values for s-ZMO, respectively. The valence band maximum (VBM) level can be calculated from the incident photon energy (21.2 eV) and the BE_{cutoff} and BE_{onset} values using the equation VBM = 21.2 − (E_{cutoff} − E_{onset}).[23] As Mg doping increased, the calculated VBM values for s-ZMO were 6.84, 6.83, 6.84, 6.87, and 6.86 eV. Combining the UPS data with the optical bandgap in Figure S2a, the CBM values were determined to be 3.31, 3.23, 3.17, 3.15, and 3.07 eV. When the QD-LEDs with s-ZMO (0–20) as the ETL were fabricated and measured, the current density per unit applied voltage (V) decreased as the Mg concentration increased. The EQE in the device incorporating s-ZMO (0–15) increased owing to the elevation of the CBM and reduced electron mobility,[37,38] resulting in an overall decrease in current density, as shown in Figure 5c. However, for s-ZMO 20, the EQE decreased owing to the excessive suppression of electron mobility (maximum EQE (%): s-ZnO: 1.13; s-ZMO 5: 1.33; s-ZMO 10: 1.76; s-ZMO 15: 2.07; and s-ZMO 20: 1.59). As the efficiency of the s-ZMO device decreased, the maximum luminance also significantly decreased relative to that of s-ZnO (73.6% reduction compared with s-ZnO) (maximum luminance (cd/m^2): s-ZnO: 19,010; s-ZMO 5: 18,297; s-ZMO 10: 17,469; s-ZMO 15: 17,492; and s-ZMO 20: 13,992) (Figure 5c,d). For comparison with s-ZMO, h-ZMO was applied to the devices, and results similar to those for s-ZMO were obtained, as shown in Figure S5. As the Mg concentration increased, the

https://doi.org/10.1021/acsanm.4c00820
ACS Appl. Nano Mater. 2024, 7, 11274−11284

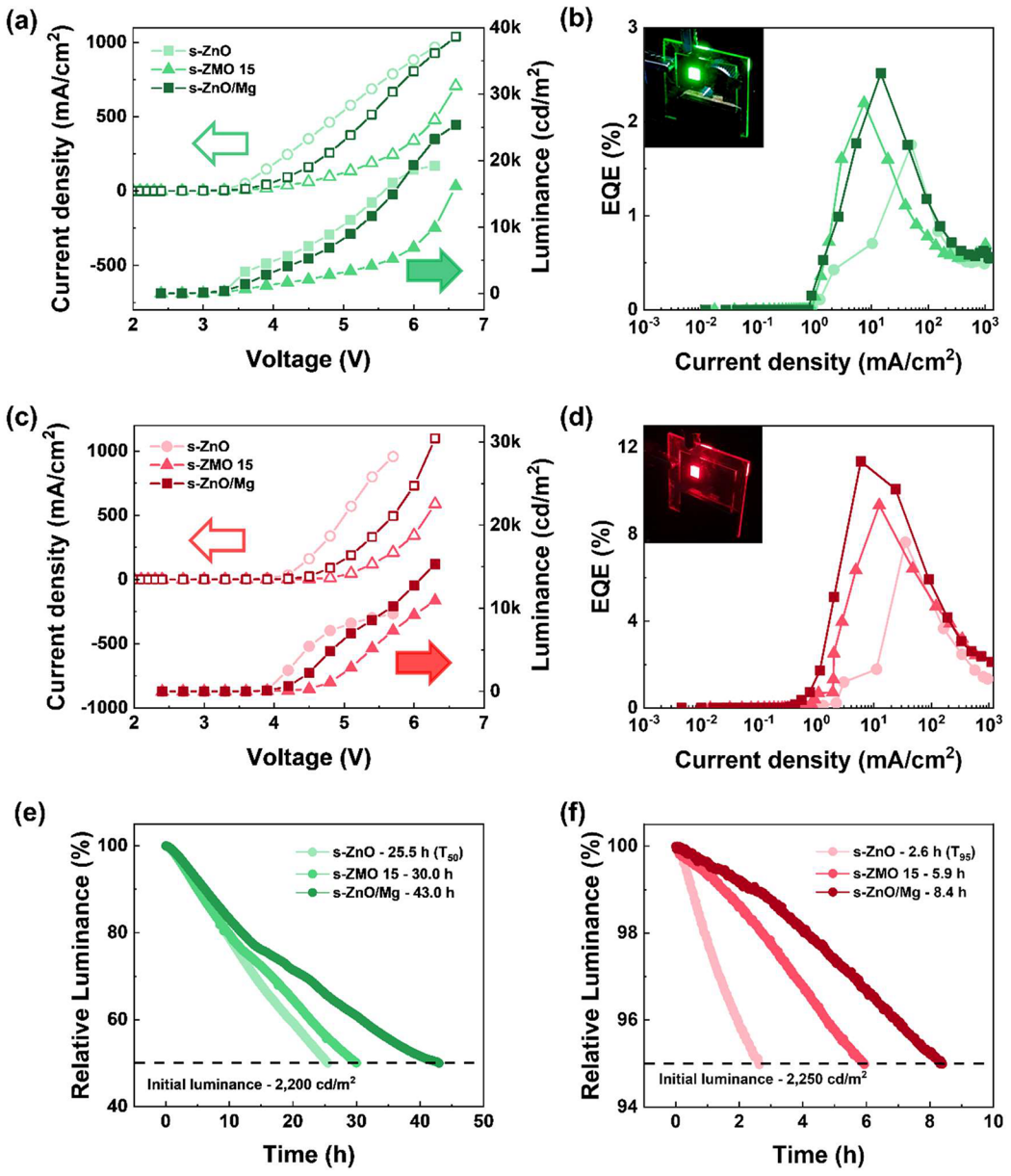

Figure 6. (a) *J*−*V*−*L* characteristics, (b) EQE−current density, and (e) device lifetime at the initial luminance of 2,200 cd/m^2 of green-emitting InP QD-LED device with s-ZnO, s-ZMO 15, and s-ZnO/Mg. (c) *J*−*V*−*L* characteristics, (d) EQE−current density device, and (f) lifetime at the initial luminance of 2,250 cd/m^2 of red-emitting InP QD-LED device with s-ZnO, s-ZMO 15, and s-ZnO/Mg.

EQE increased and current density decreased (maximum EQE (%): h-ZnO: 1.27; h-ZMO 10: 1.39; and h-ZMO 15: 1.50), whereas the maximum luminance did not change significantly (maximum luminance (cd/m^2): h-ZnO: 15,296; h-ZMO 10: 17,423; and h-ZMO 15: 15,830). s-ZnO and h-ZnO synthesized by using ultrasonic- and heating-assisted methods were compared. s-ZMO exhibited a higher current density despite its high energy level for small particles. s-ZnO exhibited more oxygen vacancies than h-ZnO, which led to an increase in the number of free electrons in ZnO, enhancing the current flow.

Although Mg doping in ZMO successfully enhanced the EL performance, notable progress is yet to be achieved in terms of TRPL. Recently, researchers aiming to mitigate defects in ZnO have explored $Mg(OH)_2$ on the ZnO surface, which reduces the impact of QDs on the ZnO interface.[28,39] Moreover, according to one study, ZMO exists in an unstable state and is susceptible to electron stress.[40,41] Therefore, to improve the stability of ZMO as an ETL, it was synthesized through ultrasonic treatment by forming $Mg(OH)_2$ on the surface of ZnO. ZnO was initially obtained and then treated with $Mg(OH)_2$ on their surfaces. The synthesis process was similar to that of s-ZnO; however, after a 20 min ultrasonic process, a Mg precursor in ethanol was added without further Zn precursor, followed by another 30 min of the ultrasonic process (Figure S6a). To investigate the particle changes during the synthesis of the Mg-treated ZnO NPs (s-ZnO/Mg), the absorbance of the solution was measured after the addition of the Mg precursor and ultrasonic processing of the ZnO precursor for 10 and 20 min (Figure S6b). When the absorption spectra of s-ZnO subjected to sonication for 10 and 20 min were compared, no noticeable changes were observed. This suggests that the growth of the ZnO NPs was complete during the 20 min ultrasonic synthesis process.

https://doi.org/10.1021/acsanm.4c00820
ACS Appl. Nano Mater. 2024, 7, 11274−11284

However, upon the addition of Mg and subsequent ultrasonic synthesis, a slight blue-shift in the absorption spectra was observed. It indicates that Mg particles form on the already formed ZnO surface, increasing the energy level through the formation of a ZMO alloy.[33] XPS analysis of s-ZnO/Mg was conducted, and the increased peak in the Mg 1s region confirmed the successful formation of Mg in s-ZnO/Mg. Additionally, TEM analysis showed that despite the formation of Mg, the average diameter (3.50 nm) and standard deviation (0.49) for s-ZnO/Mg were similar to those for s-ZnO (3.50 nm and 0.52) (Figure S6d). This suggests that the addition of $Mg(OH)_2$ has little to no impact on the particle size. When analyzing the Mg content of the s-ZnO/Mg sample through energy-dispersive X-ray spectroscopy (EDS) analysis, a Mg ratio of 8.4 mol % was confirmed. Additionally, when the Mg ratio of the s-ZMO 15 sample was examined via EDS, it was approximately 9.1 mol %, which showed a slight discrepancy compared to the Mg ratio confirmed through XPS analysis (Table S4).

To assess the effect of s-ZnO/Mg on the QD interface, TRPL measurements were conducted after the deposition of green- and red-emitting InP QD films. For comparison, measurements were performed on s-ZnO and s-ZMO 15 (Figure S7a,b). Unexpectedly, both green-emitting and red-emitting InP QD samples exhibited lower PL lifetime in s-ZnO/Mg-applied samples compared to those with a different ETL layer (green-emitting InP QD average PL lifetime τ (ns): reference: 14.53; s-ZnO: 5.42; s-ZMO 15: 5.59; s-ZnO/Mg: 4.87; and red-emitting InP QD average PL lifetime τ (ns): reference: 17.98; s-ZnO: 9.21; s-ZMO 15: 9.01; s-ZnO/Mg: 8.56) (Figure S7a,b). When analyzing the O 1s peak in the PL and XPS spectra, an elevated defect peak was observed for s-ZnO/Mg compared to s-ZnO (Figure S7c,d). Furthermore, unlike ZMO, $Mg(OH)_2$ is anticipated to form on the surface of s-ZnO/Mg. The hydroxides on this surface, acting as the cause of exciton quenching in QDs, would have exerted a more significant influence. To investigate its influence on the QD-EL, s-ZnO/Mg was applied as an ETL layer in a green-emitting InP QD EL device, and s-ZnO and s-ZMO 15 with the highest EL performance were also applied. The current density per voltage of s-ZnO/Mg showed an intermediate value between those of s-ZnO and s-ZMO 15, with a maximum luminance of 25,396 cd/m^2, which was higher than those of the QD-LED devices with s-ZnO and s-ZMO 15 (maximum luminance (cd/m^2): s-ZnO: 19184; s-ZMO 15: 16,135; and s-ZnO/Mg: 25,396) (Figure 6a). Moreover, s-ZnO/Mg exhibited the highest efficiency (maximum EQE (%): s-ZnO: 1.76; s-ZMO 15: 2.20; and s-ZnO/Mg: 2.51) (Figure 6b). Similar results were obtained when applied to a red-emitting InP QD (maximum luminance: s-ZnO: 9,342; s-ZMO 15: 10,924; and s-ZnO/Mg: 15,302) (maximum EQE (%): s-ZnO: 7.63; s-ZMO 15: 9.34; and s-ZnO/Mg: 11.35) (Figure 6c,d). Similar to the QD-EL devices incorporating s-ZMO and h-ZMO, the PL characteristics of the QD slightly influenced the EL devices. The lifetimes of green-emitting InP QD EL devices were measured. Under the conditions of s-ZnO, s-ZMO 15, and s-ZnO/Mg, the initial luminance was 2,200 cd/m^2, and T_{50} was measured until reaching 50% luminance. s-ZnO/Mg demonstrated the highest stability in the EL lifetime, with approximately 43.0 h, surpassing s-ZnO (25.5 h) and s-ZMO 15 (30.0 h) (Figure 6e). When measuring the lifetime of the red-emitting InP QD EL device, s-ZnO/Mg exhibited the highest durability, reaching T_{95} from the starting point of 2,250 cd/m^2 in 8.4 h, followed by s-ZnO 15 at 2.6 h and s-ZMO at 5.9 h. Additionally, when fitting the T_{50} value for the green device and the T_{95} value for the red device at 100 cd/m^2 with the empirical equation $Ln \times T_{50}$ = constant (L: initial luminance; n: acceleration factor), T_{50} for the green device was approximately 4,189 h and T_{95} for the red device was around 2,361 h. This record of green-emitting InP QD EL represents the highest reported lifetime among green-emitting Cd-free QD-EL devices incorporating a ZMO (Table S5). The rationale behind the enhanced stability of the s-ZnO/Mg device was substantiated using an electron-only device (EOD) structure. The EOD structure was fabricated using an ITO/ETL/InP/ETL/Ag configuration. Figure S7e shows the $J-V$ characteristics of the EOD devices with s-ZnO, s-ZMO 15, and s-ZnO/Mg as the ETL. Compared with s-ZnO, both s-ZMO 15 and s-ZnO/Mg exhibited a decrease in the current density with respect to the voltage. Additionally, when a constant current density (55.56 mA/cm^2) was applied to the EOD device and the changing voltage was represented as a function of lifetime, s-ZnO and s-ZnO/Mg exhibited an increasing trend in voltage over time as the device was damaged by the electrical current, whereas s-ZnO/Mg showed a smaller change than s-ZnO (s-ZnO: 0.104 V/h; s-ZnO/Mg: 0.056 V/h). However, for s-ZMO 15, the voltage exhibited a decreasing trend over time (s-ZMO 15: −0.222 V/h) (Figure S7f). Kwon et al. attributed the instability of ZMO to electrical stress, suggesting that the oxygen vacancies and hydroxyl bonds undergo transformation over time.[40,41] Unlike s-ZMO, s-ZnO/Mg, formed by initially synthesizing ZnO followed by coating with $Mg(OH)_2$, could alleviate the instability caused by electrical stress.

CONCLUSIONS

The absorption spectra and TEM analyses showed that the ultrasonic synthesis of ZMO nanoparticles resulted in smaller and more uniform particle sizes and higher optical energy levels compared to conventional heating methods. The XPS and PL spectra revealed a higher Mg doping ratio and fewer particle defects in s-ZMO compared with h-ZMO. When s-ZMO was applied as the ETL layer in a QD-LED, except for the s-ZMO 20 sample, a higher device performance efficiency was obtained with increasing Mg content. Additionally, utilizing the excellent Mg doping characteristics of ultrasonic synthesis, a synthesis process was performed by initially forming ZnO and subsequently coating the surface with $Mg(OH)_2$. In the case of synthesized s-ZnO/Mg nanoparticles, despite the increase in surface defects, the EL structure showed a higher EQE and luminance and demonstrated a very stable luminescence lifetime. This stability, unlike ZMO, confirmed that s-ZnO/Mg was stable under electrical stress, as evidenced by the EOD lifetime.

METHODS

Materials. Indium acetate (99.99%), zinc acetate (99.99%), TOA (98%), selenium (Se, 99.99%), sulfur (S, 99.98%), and hydrofluoric acid (HF, 48%) were purchased from Sigma-Aldrich. Oleic acid OA (99%), TOP (97%), and stearic acid (99%) were purchased from Alfa Aesar. Tris(trimethylsilyl)phosphine (TMS 3P, 99.9%) was purchased from Uniam. All chemicals were used as received. Zinc acetate dihydrate (≥98%), magnesium acetate tetrahydrate (≥98%), and potassium hydroxide (KOH) (90%, flakes) were purchased from Sigma-Aldrich, and anhydrous ethyl alcohol (99.5%) was purchased from DAEJUNG.

https://doi.org/10.1021/acsanm.4c00820
ACS Appl. Nano Mater. 2024, 7, 11274−11284

Precursor Preparation. A zinc oleate stock solution [$Zn(OA)_2$] was prepared by reacting 20 mmol of zinc acetate with 40 mmol of OA in TOA at 120 °C under a vacuum. A zinc stearate stock solution [$Zn(St)_2$] was prepared by mixing 5 mmol of zinc stearate with 10 mL of ODE. An indium laurate stock solution [$In(LA)_3$] was prepared by reacting 10 mmol of indium acetate and 30 mmol of lauric acid in an ODE at 120 °C under vacuum. Trioctylphosphine selenide (TOPSe) and trioctylphosphine sulfide (TOPS) stock solutions were prepared by reacting 20 mmol of Se or S with 10 mL of TOP at 120 °C under N_2.

Synthesis of Red InP Core/Shell QDs. Red InP core QDs were prepared as described by Choi et al.[43] InP QDs (400 nmol) and TOA (20 mL) were placed in a 100 mL round-bottomed flask and degassed at 120 °C for 1 h. After filling with N_2, 2 mL of $Zn(OA)_2$ was injected, and the temperature was increased to 340 °C. After 10 min, 0.8 mmol of diluted HF in acetone was injected, and the temperature was quenched to 120 °C. After cooling, 0.4 mL of TOPSe was injected, and the temperature was increased to 250 °C. After 2 h, the temperature was increased to 340 °C. After 30 min, 10 mL of $Zn(OA)_2$, 4 mL of TOP, and 2 mL of TOPSe were injected at a rate of 10 mL/h. After 1 h, the injection rate was decreased to 6 mL/h. After 1 h, 2.2 mL of $Zn(OA)_2$ and 0.55 mL of TOPS were then injected. After 30 min, the reaction was terminated to obtain red InP/ZnSe/ZnS core−shell QDs with a diameter of ∼11 nm. The crude solution was purified five times via a precipitation/redispersion procedure using acetone/toluene. The final purified product was redispersed in octane for storage.

Synthesis of Green InP Core/Shell QDs. Green InP-core QDs were prepared as previously described, with minor modifications.[42] In a 250 mL round-bottom flask, 20 mL of $In(LA)_3$, 20 mL of $Zn(St)_2$, and 10 mL of ODE were loaded and degassed at 150 °C. After backfilling with N_2, 10 mL of TOP and 5 mmol of $(TMS)_3P$ were added consecutively. After 5 min, the reactor was heated to 240 °C and annealed for 10 min. The same annealing protocol was performed at 280 °C for 10 min. At the end of the reaction, the reactor was cooled to room temperature. The product was purified twice with acetone and toluene using a precipitation/redispersion procedure. The final product was stored in octane. For shell formation, 290 nmol of green InP QDs and 15 mL of TOA were loaded into a 100 mL round-bottom flask and degassed at 120 °C for 1 h. After the backfilling with N_2, 0.4 mmol of diluted HF in acetone was injected. Immediately, 1.5 mL of $Zn(OA)_2$, 0.2 mL of TOPSe, and 0.1 mL of TOPS were supplied to the reactor and annealed at 230 °C for 30 min to introduce the ZnSeS molecular layer.[43] To grow ZnSeS and ZnS shells, 15 mL of $Zn(OA)_2$, 0.3 mL of TOPSe, and 0.3 mL of TOPS were added to the QD solution and reacted for 40 min at 340 °C, yielding green InP/ZnSeS/ZnS QDs with a diameter of ∼7 nm. The final product was purified five times using acetone/toluene and stored in octane until further use.

Synthesis of s-ZMO and s-ZnO/Mg NPs by the Ultrasonic Method. s-ZMO NPs were synthesized in ethanol using an ultrasonic-assisted method with an ultrasonic cleaner bath (NXPC-B5020S: 40 kHz, 200 W, and 10 L of water). Zinc acetate dihydrate and magnesium acetate tetrahydrate were added to ethyl alcohol (40 mL). Additionally, potassium hydroxide (KOH) was added to 20 mL of ethyl alcohol, and both solutions were heated to 70 °C. After mixing the two solutions and achieving transparency, the synthesis was conducted using an ultrasonic method for 20 min. In the case of s-ZnO/Mg synthesis, 0.257 g (1.2 mmol) of magnesium acetate tetrahydrate dissolved in 10 mL of ethyl alcohol was added to the synthesized solution and sonicated for 30 min. To precipitate the powder, *n*-hexane was added as an antisolvent in a 1:3 ratio. The resulting mixture underwent two rounds of washing using ethyl alcohol and *n*-hexane. Drying was performed to remove the solvent and impurities, resulting in a purified powder. The purified powder was dissolved in ethyl alcohol, and ethanolamine was added as a stabilizer.

QD-LED Fabrication. The patterned ITO glass substrate was cleaned via sonication in isopropyl alcohol (IPA). After being cleaned, the substrates were exposed to oxygen plasma for 1 min. Subsequently, PEDOT:PSS (HIL) was spin-coated onto the substrate at 3000 rpm for 30 s, and a bake was conducted at 120 °C for 10 min. The substrate was transferred to an N_2-filled glovebox and baked at 150 °C for 30 min. Subsequently, the TFB (HTL) was dissolved in *m*-xylene to a concentration of 8 mg/mL. It was then spin-coated at 4000 rpm for 30 s and baked at 150 °C for 30 min. InP QDs (EML), dissolved in octane at a concentration of 15 mg/mL, were spin-coated at 3000 rpm for 30 s and baked at 130 °C for 30 min. ZMO NPs (ETL) dissolved in ethanol at a concentration of 20 mg/mL were spin-coated at 2000 rpm for 30 s and baked at 110 °C for 30 s. Ag (cathode) was deposited to a thickness of approximately 100 nm by using a thermal evaporator. The completed substrate was encapsulated by using Norland Optical Adhesive (NOA) 8610 B epoxy.

Characterization and Analysis. The PL spectra of ZMO were obtained by using a Horiba FluoroMax Plus-C spectrofluorometer. Absorbance was measured by using a DH-2000-BAL light source. The NP size of ZMO was confirmed through TEM analysis using a JEM-2100F instrument (JEOL). XPS and UPS were conducted by using a Nexsa instrument (Thermo Fisher Scientific). Current density, luminance, and EQE of the QD-LED device were measured by using a CS-2000 spectroradiometer (Konica Minolta) and a Keithley 2400B. TRPL of ZMO was measured by time-correlated single-photon counting.

■ ASSOCIATED CONTENT

Supporting Information

The Supporting Information is available free of charge at https://pubs.acs.org/doi/10.1021/acsanm.4c00820.

Photographs of ZMO synthesis, Tauc plot for ZMO, Zn 2p and Mg 1s XPS spectra of ZMO, UPS spectra of ZMO, QD-LED device characteristics of h-ZMO and s-ZnO, schematics for s-ZnO/Mg synthesis and absorbance during the synthesis process, TRPL, PL, XPS spectra, EOD *J*−*V* characteristics and lifetime of s-ZnO/Mg, tables of elemental composition, average PL lifetime of ZMO, and performance comparison with other green-emitting InP QD-LEDs (PDF)

■ AUTHOR INFORMATION

Corresponding Author

Seong-Yong Cho − *Department of Photonics and Nanoelectronics, Hanyang University ERICA, Ansan 15588, Korea; BK21 FOUR ERICA-ACE Center, Hanyang University ERICA, Ansan 15588, Korea;* orcid.org/0000-0001-6948-171X; Email: seongyongcho@hanyang.ac.kr

Authors

Hyeonseung Ban − *Department of Photonics and Nanoelectronics, Hanyang University ERICA, Ansan 15588, Korea*

Yeongho Choi − *Department of Energy Science and Center for Artificial Atoms, Sungkyunkwan University (SKKU), Suwon 16419, Korea; SKKU Institute of Energy Science and Technology (SIEST), Sungkyunkwan University (SKKU), Suwon 16419, Korea*

Hyo Geun Lee − *Department of Photonics and Nanoelectronics, Hanyang University ERICA, Ansan 15588, Korea*

Woon Ho Jung − *Department of Energy Science and Center for Artificial Atoms, Sungkyunkwan University (SKKU), Suwon 16419, Korea; SKKU Institute of Energy Science and Technology (SIEST), Sungkyunkwan University (SKKU), Suwon 16419, Korea*

Jaehoon Lim − *Department of Energy Science and Center for Artificial Atoms, Sungkyunkwan University (SKKU), Suwon*

https://doi.org/10.1021/acsanm.4c00820
ACS Appl. Nano Mater. 2024, 7, 11274−11284

16419, Korea; SKKU Institute of Energy Science and Technology (SIEST), Sungkyunkwan University (SKKU), Suwon 16419, Korea; orcid.org/0000-0003-2623-3550

Complete contact information is available at: https://pubs.acs.org/10.1021/acsanm.4c00820

Notes

The authors declare no competing financial interest.

■ ACKNOWLEDGMENTS

This study was supported by a National Research Foundation (NRF) grant funded by the Korean Government (MSIT) (NRF-2021M3H4A3A01062964 and NRF-2022R1A4A3018802). This work was supported by a research fund from Hanyang University (HY-2023-00000000516). This research was supported by a Korea Basic Science Institute (National Research Facilities and Equipment Center) grant funded by the Ministry of Education (2021R1A6C101A405). Following are also results of a study on the "Leaders in INdustry-university Cooperation 3.0" Project, supported by the Ministry of Education and National Research Foundation of Korea.

■ REFERENCES

(1) Shirasaki, Y.; Supran, G. J.; Bawendi, M. G.; Bulović, V. Emergence of Colloidal Quantum-Dot Light-Emitting Technologies. *Nat. Photonics* **2013**, *7*, 13.

(2) Jiang, Y.; Cho, S.-Y. Y.; Shim, M. Light-Emitting Diodes of Colloidal Quantum Dots and Nanorod Heterostructures for Future Emissive Displays. *J. Mater. Chem. C Mater.* **2018**, *6* (11), 2618−2634.

(3) Pietryga, J. M.; Park, Y.-S.; Lim, J.; Fidler, A. F.; Bae, W. K.; Brovelli, S.; Klimov, V. I. Spectroscopic and Device Aspects of Nanocrystal Quantum Dots. *Chem. Rev.* **2016**, *116* (18), 10513−10622.

(4) Colvin, V. L.; Schlamp, M. C.; Alivisatos, A. P. Light-Emitting Diodes Made from Cadmium Selenide Nanocrystals and a Semiconducting Polymer. *Nature* **1994**, *370* (6488), 354−357.

(5) Dabbousi, B. O.; Bawendi, M. G.; Onitsuka, O.; Rubner, M. F. Electroluminescence from CdSe Quantum-dot/Polymer Composites. *Appl. Phys. Lett.* **1995**, *66* (11), 1316−1318.

(6) Qian, L.; Zheng, Y.; Xue, J.; Holloway, P. H. Stable and Efficient Quantum-Dot Light-Emitting Diodes Based on Solution-Processed Multilayer Structures. *Nat. Photonics* **2011**, *5* (9), 543−548.

(7) Dai, X.; Zhang, Z.; Jin, Y.; Niu, Y.; Cao, H.; Liang, X.; Chen, L.; Wang, J.; Peng, X. Solution-Processed, High-Performance Light-Emitting Diodes Based on Quantum Dots. *Nature* **2014**, *515*, 96.

(8) Janssen, R. A. J.; Stouwdam, J. W. Red, Green, and Blue Quantum Dot LEDs with Solution Processable ZnO Nanocrystal Electron Injection Layers. *J. Mater. Chem.* **2008**, *18* (16), 1889−1894.

(9) Kwak, J.; Bae, W. K.; Lee, D.; Park, I.; Lim, J.; Park, M.; Cho, H.; Woo, H.; Yoon, D. Y.; Char, K.; Lee, S.; Lee, C. Bright and Efficient Full-Color Colloidal Quantum Dot Light-Emitting Diodes Using an Inverted Device Structure. *Nano Lett.* **2012**, *12* (5), 2362−2366.

(10) Won, Y. H.; Cho, O.; Kim, T.; Chung, D. Y.; Kim, T.; Chung, H.; Jang, H.; Lee, J.; Kim, D.; Jang, E. Highly Efficient and Stable InP/ZnSe/ZnS Quantum Dot Light-Emitting Diodes. *Nature* **2019**, *575* (7784), 634−638.

(11) Kim, T.; Kim, K.-H.; Kim, S.; Choi, S.-M.; Jang, H.; Seo, H.-K.; Lee, H.; Chung, D.-Y.; Jang, E. Efficient and Stable Blue Quantum Dot Light-Emitting Diode. *Nature* **2020**, *586* (7829), 385−389.

(12) Oh, N.; Kim, B. H.; Cho, S. Y.; Nam, S.; Rogers, S. P.; Jiang, Y.; Flanagan, J. C.; Zhai, Y.; Kim, J. H.; Lee, J.; Yu, Y.; Cho, Y. K.; Hur, G.; Zhang, J.; Trefonas, P.; Rogers, J. A.; Shim, M. Double-Heterojunction Nanorod Light-Responsive LEDs for Display Applications. *Science* **2017**, *355* (6325), 616−619.

(13) Cho, S.-Y.; Oh, N.; Nam, S.; Jiang, Y.; Shim, M. Enhanced Device Lifetime of Double-Heterojunction Nanorod Light-Emitting Diodes. *Nanoscale* **2017**, *9* (18), 6103−6110.

(14) Lee, J. Y.; Kim, E. A.; Choi, Y.; Han, J.; Hahm, D.; Shin, D.; Bae, W. K.; Lim, J.; Cho, S. Y. High-Resolution Multicolor Patterning of InP Quantum Dot Films by Atomic Layer Deposition of ZnO. *ACS Photonics* **2023**, *10* (8), 2598−2607.

(15) Kim, G. H.; Lee, J.; Lee, J. Y.; Han, J.; Choi, Y.; Kang, C. J.; Kim, K. B.; Lee, W.; Lim, J.; Cho, S. Y. High-Resolution Colloidal Quantum Dot Film Photolithography via Atomic Layer Deposition of ZnO. *ACS Appl. Mater. Interfaces* **2021**, *13* (36), 43075−43084.

(16) Park, Y.-S.; Bae, W. K.; Pietryga, J. M.; Klimov, V. I. Auger Recombination of Biexcitons and Negative and Positive Trions in Individual Quantum Dots. *ACS Nano* **2014**, *8* (7), 7288−7296.

(17) Bae, W. K.; Park, Y. S.; Lim, J.; Lee, D.; Padilha, L. A.; McDaniel, H.; Robel, I.; Lee, C.; Pietryga, J. M.; Klimov, V. I. Controlling the Influence of Auger Recombination on the Performance of Quantum-Dot Light-Emitting Diodes. *Nat. Commun.* **2013**, *4*, 2661.

(18) Lee, H.; Jeong, B. G.; Bae, W. K.; Lee, D. C.; Lim, J. Surface State-Induced Barrierless Carrier Injection in Quantum Dot Electroluminescent Devices. *Nat. Commun.* **2021**, *12* (1), 5669.

(19) Rhee, S.; Chang, J. H.; Hahm, D.; Kim, K.; Jeong, B. G.; Lee, H. J.; Lim, J.; Char, K.; Lee, C.; Bae, W. K. positive Incentive" Approach to Enhance the Operational Stability of Quantum Dot-Based Light-Emitting Diodes. *ACS Appl. Mater. Interfaces* **2019**, *11* (43), 40252−40259.

(20) Lim, J.; Jeong, B. G.; Park, M.; Kim, J. K.; Pietryga, J. M.; Park, Y.-S.; Klimov, V. I.; Lee, C.; Lee, D. C.; Bae, W. K. Influence of Shell Thickness on the Performance of Light-Emitting Devices Based on CdSe/Zn1-XCdXS Core/Shell Heterostructured Quantum Dots. *Adv. Mater.* **2014**, *26* (47), 8034−8040.

(21) Kim, H.-M.; Cho, S.; Kim, J.; Shin, H.; Jang, J. Li and Mg Co-Doped Zinc Oxide Electron Transporting Layer for Highly Efficient Quantum Dot Light-Emitting Diodes. *ACS Appl. Mater. Interfaces* **2018**, *10* (28), 24028−24036.

(22) Kim, H. H.; Kumi, D. O.; Kim, K.; Park, D.; Yi, Y.; Cho, S. H.; Park, C.; Ntwaeaborwa, O. M.; Choi, W. K. Optimization of the Electron Transport in Quantum Dot Light-Emitting Diodes by Codoping ZnO with Gallium (Ga) and Magnesium (Mg). *RSC Adv.* **2019**, *9* (55), 32066−32071.

(23) Kim, J.-H.; Han, C.-Y.; Lee, K.-H.; An, K.-S.; Song, W.; Kim, J.; Oh, M. S.; Do, Y. R.; Yang, H. Performance Improvement of Quantum Dot-Light-Emitting Diodes Enabled by an Alloyed ZnMgO Nanoparticle Electron Transport Layer. *Chem. Mater.* **2015**, *27* (1), 197−204.

(24) Jing, J.; Lin, L.; Yang, K.; Hu, H.; Guo, T.; Li, F. Highly Efficient Inverted Quantum Dot Light-Emitting Diodes Employing Sol-Gel Derived Li-Doped ZnO as Electron Transport Layer. *Org. Electron* **2022**, *103*, 106466.

(25) Xiong, H.-M.; Shchukin, D. G.; Möhwald, H.; Xu, Y.; Xia, Y.-Y. Sonochemical Synthesis of Highly Luminescent Zinc Oxide Nanoparticles Doped with Magnesium(II). *Angew. Chem., Int. Ed.* **2009**, *48* (15), 2727−2731.

(26) Chrzanowski, M.; Kuchowicz, M.; Szukiewicz, R.; Sitarek, P.; Misiewicz, J.; Podhorodecki, A. Enhanced Efficiency of Quantum Dot Light-Emitting Diode by Sol-Gel Derived $Zn_{1-x}Mg_xO$ Electron Transport Layer. *Org. Electron* **2020**, *80*, 105656.

(27) Alexandrov, A.; Zvaigzne, M.; Lypenko, D.; Nabiev, I.; Samokhvalov, P. Al-, Ga-, Mg-, or Li-Doped Zinc Oxide Nanoparticles as Electron Transport Layers for Quantum Dot Light-Emitting Diodes. *Sci. Rep* **2020**.

(28) Han, C.-Y.; Lee, S.-H.; Song, S.-W.; Yoon, S.-Y.; Jo, J.-H.; Jo, D.-Y.; Kim, H.-M.; Lee, B.-J.; Kim, H.-S.; Yang, H. More Than 9% Efficient ZnSeTe Quantum Dot-Based Blue Electroluminescent Devices. *ACS Energy Lett.* **2020**, *5* (5), 1568−1576.

(29) Jo, C.-S.; Noh, K.; Noh, S. H.; Yoo, H.; Kim, Y.; Jang, J.; Lee, H. H.; Jung, Y.-J.; Lee, J.-H.; Han, J.; Lim, J.; Cho, S.-Y. Solution-Processed Fabrication of Light-Emitting Diodes Using CsPbBr3

Perovskite Nanocrystals. *ACS Appl. Nano Mater.* **2020**, *3* (12), 11801−11810.
(30) Sun, D.; Wong, M.; Sun, L.; Li, Y.; Miyatake, N.; Sue, H.-J. Purification and Stabilization of Colloidal ZnO Nanoparticles in Methanol. *J. Solgel Sci. Technol.* **2007**, *43* (2), 237−243.
(31) Noh, K.; Kim, M.; Lee, S. H.; Yun, H. S.; Lim, T. H.; Choi, Y.; Kim, K. J. B.; Jiang, Y.; Beom, K.; Kim, M.; Kim, Y. G.; Lee, P.; Oh, N.; Kim, B. H.; Shin, C.; Lee, H. H.; Yoon, T.-S.; Shim, M.; Lim, J.; Kim, K.-B.; Cho, S. Y. Effect of Ethanolamine Passivation of ZnO Nanoparticles in Quantum Dot Light Emitting Diode Structure. *Curr. Appl. Phys.* **2019**, *19* (9), 998−1005.
(32) Coulter, J. B.; Birnie III, D. P. Assessing Tauc Plot Slope Quantification: ZnO Thin Films as a Model System. *physica status solidi (b)* **2018**, *255* (3), 1700393.
(33) Hou, Y.; Mei, Z.; Du, X. Semiconductor Ultraviolet Photodetectors Based on ZnO and MgxZn1-xO. *J. Phys. D Appl. Phys.* **2014**, *47* (28), 283001.
(34) Moyen, E.; Kim, J. H.; Kim, J.; Jang, J. ZnO Nanoparticles for Quantum-Dot-Based Light-Emitting Diodes. *ACS Appl. Nano Mater.* **2020**, 3 (6), 5203−5211.
(35) Li, S.-S.; Su, Y.-K. Improvement of the Performance in Cr-Doped ZnO Memory Devices via Control of Oxygen Defects. *RSC Adv.* **2019**, *9* (6), 2941−2947.
(36) Pal, A.; Srivastava, S.; Saini, P.; Raina, S.; Ingole, P. P.; Gupta, R.; Sapra, S. Probing the Mechanism of Fluorescence Quenching of QDs by Co(III)-Complexes: Size of QD and Nature of the Complex Both Dictate Energy and Electron Transfer Processes. *J. Phys. Chem. C* **2015**, *119* (39), 22690−22699.
(37) Yarar, Z. Steady-State Electron Transport and Low-Field Mobility of Wurtzite Bulk ZnO and Zn1-xMgxO. *J. Electron. Mater.* **2011**, *40* (4), 466−472.
(38) Cohen, D. J.; Ruthe, K. C.; Barnett, S. A. Transparent Conducting Zn1-xMgxO:(Al,In) Thin Films. *J. Appl. Phys.* **2004**, *96* (1), 459−467.
(39) Ning, M.; Cao, S.; Li, Q.; Luo, H.; Du, Z.; Wang, Y.; Zhao, J. Improving Performance of InP-Based Quantum Dot Light-Emitting Diodes by Controlling Defect States of the ZnO Electron Transport Layer. *J. Phys. Chem. C* **2023**, *127* (1), 824−830.
(40) Shin, D. H.; Lampande, R.; Kim, S. J.; Jung, Y. H.; Kwon, J. H. Understanding the Origin of Degradation of InP-Quantum Dot Light-Emitting Diodes. *Adv. Electron Mater.* **2022**, *8* (10), 2200256.
(41) Mude, N. N.; Khan, Y.; Thuy, T. T.; Walker, B.; Kwon, J. H. Stable ZnS Electron Transport Layer for High-Performance Inverted Cadmium-Free Quantum Dot Light-Emitting Diodes. *ACS Appl. Mater. Interfaces* **2022**, *14* (50), 55925−55932.
(42) Kim, Y.; Ham, S.; Jang, H.; Min, J. H.; Chung, H.; Lee, J.; Kim, D.; Jang, E. Bright and Uniform Green Light Emitting InP/ZnSe/ZnS Quantum Dots for Wide Color Gamut Displays. *ACS Appl. Nano Mater.* **2019**, *2* (3), 1496−1504.
(43) Choi, Y.; Hahm, D.; Bae, W. K.; Lim, J. Heteroepitaxial Chemistry of Zinc Chalcogenides on InP Nanocrystals for Defect-Free Interfaces with Atomic Uniformity. *Nat. Commun.* **2023**, *14* (1), 43.

https://doi.org/10.1021/acsanm.4c00820
ACS Appl. Nano Mater. 2024, 7, 11274−11284